INTERNATIONAL JOURNAL OF MARITIME TECHNOLOGY
IJMT Vol.6/ Summer 2016 (31-40)

Available online at: http://ijmt.ir/browse.php?a_code=A-10-100-6&sid=1&slc_lang=en

Parametric Study on Wave Interaction with a Porous Submerged Rubble Mound Breakwater Using Modified N-S Equations and Cut-Cell Method

Saeed Booshi[1], Mohammad Javad Ketabdari[2*]

[1]MSc, Amirkabir University of Technology, Faculty of Marine Technology, saeed.booshi@aut.ac.ir
[2]Associate Professor, Amirkabir University of Technology, Faculty of Marine Technology, ketabdar@aut.ac.ir

ARTICLE INFO

Article History:
Received: 29 Aug. 2016
Accepted: 13 Feb. 2017

Keywords:
Submerged Rubble Mound Breakwater
Porous Media
Cut-Cell Porous Method
VOF Method
Transmitted Waves

ABSTRACT

In this paper wave transformation in a submerged sloped breakwater and its hydraulic performance was simulated by developing a numerical model in Fortran. The code was established by combining porous flow and a two-phase model using VOF method. Modified Navier-Stokes and k-ε equations implemented to the model to simulate the flow in porous media. Cut cell method was modified to simulate fluid transformation from sloped porous media's boundary in more accurate way and then applied in the governing equations to increase the accuracy of the model. The validity of the present program was investigated based on the comparisons with the available experimental data. The results showed that increasing of inertia coefficient and wave period and also reduction of porosity lead to some phase lags between the incident and transmitted waves. Furthermore parametric studies were performed on effect of submerged porous breakwater crest widths and heights on transmitted waves leading to useful results for design criteria.

1. Introduction

Breakwaters are usually used to provide a calm area for loading and offloading of ships or protect the shoreline by forcing the waves break and release their energy. These structures have different geometries and shapes related to their position and environmental conditions. Effect of wave motion on breakwaters and hydraulic performance of these barriers have been studied in the past few decades. Vilchez et al. [1] developed a method to evaluate the hydraulic performance resulting from the interaction of perpendicularly impinging water waves on various types of breakwater [1]. They used data obtained from physical tests in a wave flume with irregular waves. Jensen et al. [2] re-examined the porous media equations and considered new calibration cases to achieve a better understanding of the variation of the resistance coefficients. In their work constant values for the resistance coefficients for a broad range of flow conditions were recommended. Liu and Li [3] used velocity potential decompositions and the matched Eigen function expansions in the porous media to obtain a new solution for wave reflection and transmission by a surface-piercing porous breakwater with an analytical approach. They used complex dispersion relations in the porous breakwater and avoided finding complex wave numbers and handling nonself- adjoint eigenvalue problem. Yang et al. [4] used projection schemes and a finite element method on unstructured grids to solve Euler/Navier-Stokes equations for incompressible fluid in an Arbitrary Lagrangian-Eulerian (ALE) frame. They studied the effects of rubble types on the wave dissipation and wave overtopping of rubble mound breakwater. In their research to simulate the porous medium small solid blocks were used in the domain. Wu and Hsiao [5] implemented a numerical model based on the Volume-Averaged Reynolds Averaged Navier–Stokes equations (VARANS) coupled with the non-linear k–ε turbulence closure solver to simulate propagation of solitary waves over a submerged permeable breakwater. The porous medium, consisting of uniform glass spheres, was mounted on the seafloor. They used this model to estimate the reflection, transmission and dissipation of waves using the energy integral method by varying the aspect ratio and the grain size of the permeable obstacle. Hieu and Vinh [6] used a VOF-based two-phase flow model to study the interactions of waves and a seawall protected by a submerged porous structure with a permeable terrace. They concluded that the overtopping rate was strongly dependent on the energy dissipation due to the drag force. Mendez et al. [7] analyzed influence of wave reflection and energy

dissipation in the submerged porous media. For this purpose, they obtained analytical expressions for the mean quantities such as mass and energy fluxes in terms of the shape functions. Nevertheless their model seems to be unpractical for arbitrary geometries of a breakwater. Karim et al. [8, 9] modeled wave motion in porous structure using VOF method. They used VOF method to treat the free surface. In their model, the equations were applicable for only rectangular porous cells in the wall boundaries. Zhang et al. [10] developed an integrated model based on the VARANS and Biot'sporo-elastic theory to investigate the interaction of waves with a submerged permeable structure. They have studied wave behavior through a parametric study on wave and structure characteristics. Guta and Sundar [11] simulated progressive waves over rectangular porous structure using time dependent incompressible Navier-Stokes-Brinkman system. They used finite volume technique to discretize governing equations. Based on their numerical model, in the case of sloped boundaries, they had to use smaller grids and other techniques which lead to smaller time-steps. Zhao et al. [12] simulated breaking waves by multi-scale turbulent model focusing on the turbulent production and dissipation in wave breaking process. Their focus was on the performance and accuracy of turbulent models in the simulation process. Gracia et al. [13] presented a numerical model to study the wave propagation above a low crested permeable breakwater. In their work wave elevation was recorded in different points above the structure at breaking zone to investigate flow motion in the porous media. Their models had some limitations as it was applicable only for low crested structures. Hieu et al. [14] simulated breaking of linear waves in interaction with a porous submerged breakwater. They investigated hydraulic performance of this structure in interaction with waves and effect of porosity on the reflection, transmission and dissipation coefficients. Interaction of solitary and random waves with porous structures was studied by some other researchers in recent years. For example Lynett et al. [15] presented a numerical model for solitary wave interaction with vertically walled porous structures. In their research, they focused on the reflection, transmission, and diffraction of solitary waves by the porous structure. In the case of random waves, Lara et al. [16] applied RANS equations to model wave interaction with submerged permeable structures. They obtained good results for height envelopes, mean level and spectral shape of free surface displacement and dynamic pressure inside the breakwater.

The broad literature review on wave-porous media interaction in this section shows that there is no clear approach to model sloped boundaries of a porous media with sloped cells.

Therefore in this research, a VOF-based numerical solution is presented to model unsteady flow using Navier-Stokes equations. A new algorithm was developed to simulate flow through the porous media based on the Cut-Cell method to increase the performance of the model. This model was employed to simulate wave motion in porous media of a submerged breakwater. Reaction of breakwater to incident waves with different heights and periods was investigated. Special attention was then paid on the effect of rubble mound breakwater characteristics on its performance associated with damping rate and transmitted waves characteristics.

It should be noted that using the present model in which cut-cell method and porous equations were combined, unlike the other numerical works in this area there is no need to use small grid for the boundary cells of sloped side of the porous breakwater. Slope of the boundary can be easily modeled with sloped cells. This approach leads to a more efficient and faster computer code which doesn't need to use smaller time steps and more equations near the walls like wall-function method.

2. Governing Equations

In this study fluid assumed to be viscous and incompressible and so Navier-Stokes and continuity equations were used as governing equations. Extended equations were used within porous medium as [9]:

$$\frac{\partial(\gamma_y v)}{\partial y}+\frac{\partial(\gamma_z w)}{\partial z}=0 \tag{1}$$

$$\lambda_v\frac{\partial v}{\partial t}+\frac{\partial(\lambda_y v^2)}{\partial y}+\frac{\partial(\lambda_z vw)}{\partial z}+\gamma_v\frac{\partial \psi}{\partial y}=(\nu+\nu_t)\left[\frac{\partial}{\partial y}\left\{\gamma_y\left(2\frac{\partial v}{\partial y}\right)\right\}+\frac{\partial}{\partial z}\left\{\gamma_z\left(\frac{\partial v}{\partial z}+\frac{\partial w}{\partial y}\right)\right\}\right]-R_y \tag{2}$$

$$\lambda_v\frac{\partial w}{\partial t}+\frac{\partial(\lambda_y vw)}{\partial y}+\frac{\partial(\lambda_z w^2)}{\partial z}+\gamma_v\frac{\partial \psi}{\partial z}=(\nu+\nu_t)\left[\frac{\partial}{\partial y}\left\{\gamma_y\left(\frac{\partial w}{\partial y}+\frac{\partial v}{\partial z}\right)\right\}+\frac{\partial}{\partial z}\left\{\gamma_z\left(2\frac{\partial w}{\partial z}\right)\right\}\right]-R_z \tag{3}$$

In these equations t is the time, v and w are the velocity components in y and z directions respectively, ν is the kinematic molecular viscosity; ν_t is the kinematic eddy viscosity; g is the gravitational acceleration; $\psi = p/\rho + gz$ in which is the mean pressure, ρ is the fluid density, and R_y and R_z are resistance forces exerted by porous media. These are defined as:

$$R_y=\frac{1}{2}\frac{C_D}{\Delta y}(1-\gamma_y)\,v\sqrt{v^2+w^2} \tag{4}$$

$$R_z = \frac{1}{2}\frac{C_D}{\Delta z}(1-\gamma_z)\, w\sqrt{v^2+w^2} \qquad (5)$$

in which C_D is the drag coefficient, γ_v is the volumetric porosity and γ_y, γ_z are superficial porosities of breakwater. λ_v, λ_y and λ_z are defined based on these coefficients, respectively, using following relationships:

$$\lambda_v = \gamma_v + (1-\gamma_v)C_M \qquad (6)$$

$$\lambda_y = \gamma_y + (1-\gamma_y)C_M \qquad (7)$$

$$\lambda_z = \gamma_z + (1-\gamma_z)C_M \qquad (8)$$

where C_M is the inertia coefficient. It should be noted that for a cell, outside the porous medium volumetric and superficial porosities are unity, while for a cell inside the porous medium these coefficients are between zero and unity.

For a turbulent flow, modified k-ε method for porous medium was used [17]. The kinematic eddy viscosity is defined as follows:

$$\nu_t = C_\mu \frac{k^2}{\varepsilon} \qquad (9)$$

where k is the kinematic energy and ε is the energy dissipation. In this method, in order to consider dynamics of turbulent, two model equations are used. In the first equation, generation of turbulent kinematic energy and in the second one rate of viscous dissipation is considered:

$$C_\mu \frac{k^2}{\varepsilon}\lambda_v \frac{\partial k}{\partial t} + \frac{\partial(\lambda_y v k)}{\partial y} + \frac{\partial(\lambda_z w k)}{\partial z} = \frac{\partial}{\partial y}\left[\gamma_y \nu_k \left(\frac{\partial k}{\partial y}\right)\right] + \frac{\partial}{\partial z}\left[\gamma_z \nu_k \left(\frac{\partial k}{\partial z}\right)\right] - \gamma_z G_S - \gamma_v \varepsilon \qquad (10)$$

$$\lambda_v \frac{\partial \varepsilon}{\partial t} + \frac{\partial(\lambda_y v \varepsilon)}{\partial y} + \frac{\partial(\lambda_z w \varepsilon)}{\partial z} = \frac{\partial}{\partial y}\left[\gamma_y \nu_\varepsilon \left(\frac{\partial \varepsilon}{\partial y}\right)\right] + \frac{\partial}{\partial z}\left[\gamma_z \nu_\varepsilon \left(\frac{\partial \varepsilon}{\partial z}\right)\right] - \gamma_v C_1 G_S - \gamma_v C_2 \frac{\varepsilon^2}{k} \qquad (11)$$

where $C_1 = 1.44$, $C_2 = 1.92$, $\sigma_k = 1.0$, $\sigma_\varepsilon = 1.3$, $\nu_\varepsilon = \nu + \nu_t/\sigma_\varepsilon$ and G_s is a function of velocities derivatives as:

$$G_S = \nu_t\left[2\left(\frac{\partial v}{\partial y}\right)^2 + 2\left(\frac{\partial w}{\partial z}\right)^2 + \left(\frac{\partial w}{\partial y} + \frac{\partial v}{\partial z}\right)^2\right] \qquad (12)$$

In this paper behavior of free surface was simulated using VOF method. This method is based on the advection equation in which F has a specific value for each cell so that its quantity is related to position of this cell as follows:

$$\frac{\partial(\gamma_v F)}{\partial t} + \frac{\partial(\gamma_y v F)}{\partial y} + \frac{\partial(\gamma_z w F)}{\partial z} = 0 \qquad (13)$$

$$\begin{cases} F = 1 & Full\ cell \\ F = 0 & Empty\ cell \\ 0 < F < 1 & Interface\ cell \end{cases}$$

Youngs' VOF method was implemented in present model to track the free surface. In this method advection of the free surface due to velocity field is reconstructed with sloped lines. The first step of this method is to find angle of free surface cell with horizontal axis (β) that is estimated with eight neighboring cells information (Figure 1)

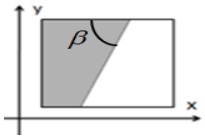

Figure 1. Angle of free surface (β) in Youngs' VOF method;

$$\beta = \tan^{-1}\left[\frac{-n^y}{n^z}\right] \qquad (-\pi < \beta \le \pi) \qquad (14)$$

where

$$n^y{}_{j,k} = \frac{\gamma_v}{\Delta y}(F_{j+1,k+1} + 2F_{j+1,k} + F_{j+1,k-1} - F_{j-1,k+1} - 2F_{j-1,k} - F_{j-1,k-1}) \qquad (15)$$

$$n^z{}_{j,k} = \frac{\gamma_v}{\Delta z}(F_{j+1,k+1} + 2F_{j,k+1} + F_{j-1,k+1} - F_{j+1,k-1} - 2F_{j,k-1} - F_{j-1,k-1}) \qquad (16)$$

Estimation of advection in this method is based on the four essential situations (Figure 2). While another twelve situations can be obtained from the conformation of these essential situations.

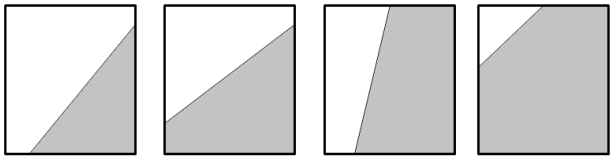

Figure 2. Four main situations for Youngs' VOF;

In this process, another angle (α) should be calculated for each cell as:

$$\alpha = \tan^{-1}\left(\frac{\delta y}{\delta z}\tan\beta\right) \qquad (0 \le \alpha \le \pi/2) \qquad (17)$$

Finally, with knowing α and F, type of each cell is determined and flux for outward velocities for each cell is calculated [18]. This process is performed in

each time step and effective values for density and viscosity are calculated as follows:

$$\rho_{eff} = F\rho_{water} + (1-F)\rho_{air} \quad (18)$$

$$\mu_{eff} = F\mu_{water} + (1-F)\mu_{air} \quad (19)$$

$$v_{eff} = \frac{\mu_{eff}}{\rho_{eff}} \quad (20)$$

3. Cut-Cell Method Implementation to the Porous Media

In this paper, partial cell method was applied for porous medium. This method was used by some researchers to consider sloped and arbitrary meshes in boundary of fluid with solid structure. Assuming flow to be incompressible and viscous Tucker and Pan [19] investigated laminar flow by this method. Lou et al. [20] simulated flow with irregular 3D domain using this method and finite volume technique. Kirkpatrick [21] et al. applied cut cell method on the staggered 3D Cartesian grid to model curved boundaries and flow around a circular rigid body. Kim et al. [22] modified this approach to simulate shallow water waves numerically. They used total variation diminishing weighted average flux method to improve accuracy of presented model.

In partial cell method for solid structures, five coefficients were considered for sloped geometry of boundaries of each cell (Figure 3) to discretize the equations. For example in solving Navier-Stokes equations with simplified marker and cell (SMAC) method, by applying theses coefficients in continuity equation's discretization, the sloped geometry is considered in staggered grid as:

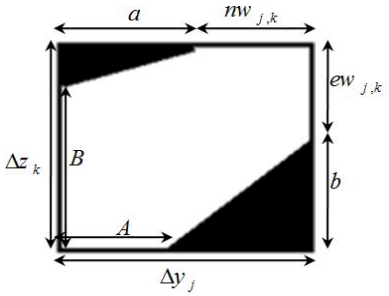

Figure 3. A mesh cell with solid walls;

$$\frac{1}{vc_{i,j}}\left[\left(ew_{j,k}v^{n+1}_{j+1/2,k} - ew_{j-1,k}v^{n+1}_{j-1/2,k}\right)/\Delta y_j + (nw_{j,k}w^{n+1}_{j,k+1/2} - nw_{j,k-1}w^{n+1}_{j,k-1/2})/\Delta z_k\right] = 0 \quad (21)$$

$$ew_{j,k} = 1.0 - (b/\Delta z_k) \quad (22)$$

$$nw_{j,k} = 1.0 - (a/\Delta y_j) \quad (23)$$

$$vc_{j,k} = 1.0 - \frac{0.5}{\Delta y \Delta z}\left[a(\Delta z - B) + b(\Delta y - A)\right] \quad (24)$$

where $vc_{j,k}$ is the non-dimensional volume of non-solid part of the mesh cell.

If one side of the cell is solid its wall coefficient would be zero. While for no solidness wall it would be unity. This idea is implemented to consider the slope of the boundaries in porous medium (Figure 4). Wall coefficients for each cell were considered as:

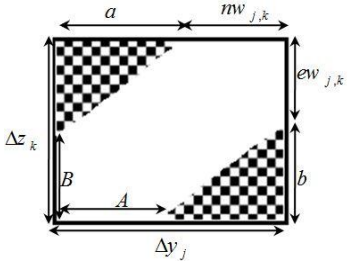

Figure 4. A mesh cell with porous walls;

$$EW_{j,k} = ew_{j,k}(\gamma_y)_f + (1.0 - ew_{j,k})(\gamma_y)_p \quad (25)$$

$$NW_{j,k} = nw_{j,k}(\gamma_z)_f + (1.0 - nw_{j,k})(\gamma_z)_p \quad (26)$$

The volume coefficient can be obtained as:

$$VC_{j,k} = vc_{j,k}(\gamma_v)_f + (1.0 - vc_{j,k})(\gamma_v)_p \quad (27)$$

$$vc_{j,k} = (\gamma_v)_f\left[1.0 - \frac{0.5}{\Delta y \Delta z}\left[a(\Delta z - B) + b(\Delta y - A)\right]\right] + (\gamma_v)_p\left[\frac{0.5}{\Delta y \Delta z}\left[a(\Delta z - B) + b(\Delta y - A)\right]\right] \quad (28)$$

According to the related coefficients for a porous cell, the advection equation was modified as follows:

$$\frac{\partial(\bar{\gamma}_v F)}{\partial t} + \frac{\partial(\bar{\gamma}_y vF)}{\partial y} + \frac{\partial(\bar{\gamma}_z wF)}{\partial z} = 0 \quad (29)$$

where the corrected coefficients are:

$$(\bar{\gamma}_v)_{j,k} = vc_{j,k}(\gamma_v)_f + (1.0 - vc_{j,k})(\gamma_v)_p \quad (30)$$

$$(\bar{\gamma}_y)_{j,k} = vc_{j,k}(\gamma_y)_f + (1.0 - vc_{j,k})(\gamma_y)_p \quad (31)$$

$$(\bar{\gamma}_z)_{j,k} = vc_{j,k}(\gamma_z)_f + (1.0 - vc_{j,k})(\gamma_z)_p \quad (32)$$

This new formulation let one to simulate free surface motion through cut-cell porous cells. We called this approach as Cut-Cell Porous method and was applied in the numerical model in this reserach. It is described in the next sections.

4. Solution Method

The staggered grid system was applied to discretize the governing equations with finite difference technique. In this grids system, pressure and viscosity are located in the center of the cell and velocity components are defined in the cell faces (Figure 5). In order to solve Navier-Stokes and continuity equations SMAC method was used [23]. The steps of this method are as follows:

a) Solve the momentum equations for V and W explicitly.
b) Solve the Poisson equation and calculate δp for the pressure corrections.
c) Adjust the pressure and velocity.
d) Return to step (b) and repeat this procedure until the continuity equation converges.
Discretization of momentum equation in y direction and also continuity equation are given here in detail. Discretization of the other equation is similar to the first one.

$$\hat{V}_{j+1/2,k} = V^{n}_{j+1/2,j} - \frac{\Delta t}{(\bar{\lambda}_v)_{j+1/2,k}} \left[-(\bar{\gamma}_v)_{j+1/2,k} \right. \qquad (33)$$

$$\left. (\Delta p^{n+1}{}_{j+1/2,k}) / \Delta y_{j+1/2} + g_y - FVY - FVZ + VISY + R_y \right]$$

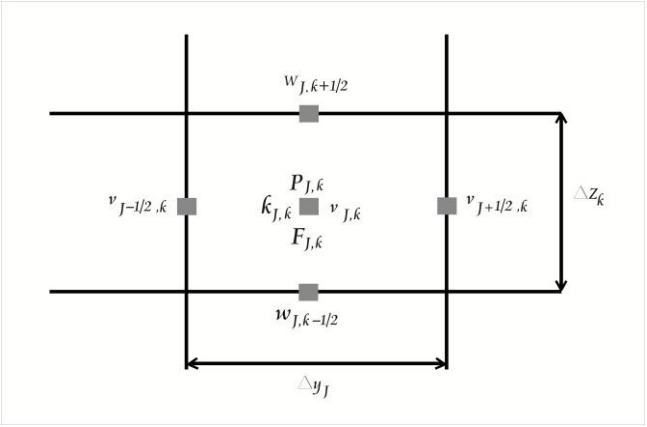

Figure 5. Set up of variables in a cell;

Corrected pressure, $\delta p = p^{n+1}_{j,k} - p^{n}_{j,k}$, was calculated by the following relationship:

$$(\bar{\gamma}_y)_{j+1/2,k} \frac{\partial^2 \delta p}{\partial y^2} + (\bar{\gamma}_z)_{j+1/2,k} \frac{\partial^2 \delta p}{\partial z^2} = \frac{(\bar{\lambda}_v)_{j+1/2,k}}{(\bar{\gamma}_v)_{j+1/2,k}} \frac{\rho}{\Delta t} \nabla_d \hat{v} \qquad (34)$$

where ∇_d denotes the discrete gradient operator. Pressure correction, δp, is used in the following relationship to modify the velocity and pressure in new time step:

$$V^{n+1}_{j+1/2,k} = \hat{v}_{j+1/2,k} - (\frac{\gamma_v}{\lambda_v})_{j+1/2,k} \rho_{j+1/2,k} \Delta t \nabla_d \delta p \qquad (35)$$

$$p^{n+1}_{j,k} = p^{n}_{j,k} + \delta p \qquad (36)$$

$$(\bar{\gamma}_v)_{j+1/2,k} = vc_{j+1/2,k} (\gamma_v)_f + (1.0 - vc_{j+1/2,k})(\gamma_v)_p \qquad (37)$$

$$(\bar{\lambda}_v)_{j+1/2,k} = vc_{j+1/2,k} (\lambda_v)_f + (1.0 - vc_{j+1/2,k})(\lambda_v)_p \qquad (38)$$

In these equations, v^n is the velocity at the previous time step; $\hat{v}$ is the temporary velocity in the new time step; *FVY* and *FVZ* are the convection fluxes in the horizontal and vertical directions respectively and *VISY* is the diffusion term:

$$FVY = (\bar{\lambda}_y)_{j+1/2,k} (V^{n}_{j+1/2,k} / \Delta y_\alpha) \left[\Delta y_{j+1}\, DVL + \Delta y_j\, DVR + \right. \qquad (39)$$

$$\left. \alpha\, \mathrm{sgn}(v^{n}_{j+1/2,k})\, (\Delta y_{j+1}\, DVL - \Delta y_j\, DVR) \right]$$

The used terms are as follows:

$$DVL = (v^{n}_{j+1/2,k} - v^{n}_{j-1/2,k}) / \Delta y_j \qquad (40)$$

$$DVR = (v^{n}_{j+3/2,k} - v^{n}_{j+1/2,k}) / \Delta y_{j+1} \qquad (41)$$

$$\Delta y_\alpha = \Delta y_{j+1} + \Delta y_j + \alpha\, \mathrm{sgn}(v^{n}_{j+1/2,k})\, (\Delta y_{j+1} - \Delta y_j) \qquad (42)$$

Convection flux in the vertical direction:

$$FVZ = (\bar{\lambda}_z)_{j+1/2,k} (\mathrm{w}^{*}_{j+1/2,k} / \Delta z_\alpha) \left[\Delta z_{k+1/2}\, DWB + \Delta z_{k-1/2} \right. \qquad (43)$$

$$\left. DWT + \alpha\, \mathrm{sgn}(\mathrm{w}^{*}_{j+1/2,k})\, (\Delta z_{k+1/2}\, DWB - \Delta z_{k-1/2}\, DWT) \right]$$

The used terms are as follows:

$$DVB = (v^{n}_{j+1/2,k} - v^{n}_{j+1/2,k-1}) / \Delta z_{k-1/2} \qquad (44)$$

$$DVT = (v^{n}_{j+1/2,k+1} - v^{n}_{j+1/2,k}) / \Delta z_{k+1/2} \qquad (45)$$

$$\mathrm{w}^{*}_{j+1/2,k} = \left[\Delta \mathrm{y}_j (\mathrm{w}^{n}_{j+1,k+1/2} + \mathrm{w}^{n}_{j+1,k-1/2}) + \right. \qquad (46)$$

$$\left. \Delta \mathrm{y}_{j+1} (\mathrm{w}^{n}_{j,k+1/2} + \mathrm{w}^{n}_{j,k-1/2}) \right] / 2(\Delta \mathrm{y}_j + \Delta \mathrm{y}_{j+1})$$

$$\Delta z_\alpha = \Delta z_{k+1/2} + \Delta z_{k-1/2} + \alpha\, \mathrm{sgn}(w^{*}_{j+1/2,k})\, (\Delta z_{k+1/2} - \Delta z_{k-1/2}) \qquad (47)$$

Diffusion term can be calculated using the following equation:

$$VISY = \frac{4}{(\Delta y_j + \Delta y_{j+1})} \left[(\bar{\gamma}_y \nu_T)_{j+1,k} DVR - (\bar{\gamma}_y \nu_T)_{j,k} DVL \right]$$

$$+ \frac{2}{\Delta z_{k-1/2} + \Delta z_{k+1/2}} \left[(\bar{\gamma}_z \nu_T)_{j+1/2,k+1/2} DVT - (\bar{\gamma}_z \nu_T)_{j+1/2,k-1/2} DVB \right] \qquad (48)$$

$$+ \frac{1}{\Delta z_k} \left[(\bar{\gamma}_z \nu_T)_{j+1/2,k+1/2} DWT - (\bar{\gamma}_z \nu_T)_{j+1/2,k-1/2} DWB \right]$$

where:

$$DWB = (w^{n}{}_{j+1,k-1/2} - w^{n}{}_{j,k-1/2}) / \Delta y_{j+1/2} \qquad (49)$$

$$DWT = (w^{n}{}_{j+1,k+1/2} - w^{n}{}_{j,k+1/2}) / \Delta y_{j+1/2} \qquad (50)$$

$$(R_y)_{j+1/2,k} = \frac{1}{2} \frac{C_D}{\Delta y_{j+1/2}} (1 - (\gamma_y)_{j+1/2,k}) \qquad (51)$$

$$v_{j+1/2,k} \sqrt{(v_{j+1/2,k})^2 + (w^{*}{}_{j+1/2,k})^2}$$

$$\frac{1}{VC_{i,j}} \left[\left(EW_{j,k}\, v^{n+1}_{j+1/2,k} - EW_{j-1,k}\, v^{n+1}_{j-1/2,k} \right) / \Delta y_j + \right. \qquad (52)$$

$$\left. (NW_{j,k} w^{n+1}_{j,k+1/2} - NW_{j,k-1} w^{n+1}_{j,k-1/2}) / \Delta z_k \right] = 0$$

After calculation of velocity and pressure field in the new time step, the advection equation of VOF function was solved based on the new velocity field using Youngs' VOF method and free surface was reconstructed. Effective values of density and viscosity were calculated for each cell in the next time step using volume of fluid method.

In order to prevent the model divergence, the Courant-Friedrichs-Levy (CFL) condition [24] and a diffusive limitation [25] were considered respectively as follows:

$$\Delta t_c = \min\left[\min\left(\frac{\Delta y_j}{|v_{j,k}|}\right), \min\left(\frac{\Delta z_k}{|w_{j,k}|}\right)\right] \tag{53}$$

$$\Delta t_v = \frac{1}{2}\left[\frac{1}{v_e\left[\left(\frac{1}{\Delta y_j}\right)^2 + \left(\frac{1}{\Delta z_k}\right)^2\right]}\right] \tag{54}$$

The minimum value of these time steps was used in the numerical model in each time step.

In the computation domain, for initial condition still water level was considered. Therefore hydrostatic pressure is initial pressure in computational cells at t=0. In top and bottom walls zero velocity was applied for vertical velocities. While Nueman boundary condition was assumed for tangential velocities. In order to generate a linear wave with an amplitude A and an angular frequency ω, in the left hand side of the Numerical Wave Tank (NWT), piston type wave maker was used (e.g. see Katell and Eric, 2002) [26]. The relations for this type of wave generation are as follows:

$$\eta = A\cos(\omega t) \tag{55}$$

$$V_{wavemaker} = \frac{2kh + \sinh 2kh}{2(\cosh 2kh\text{-}1)}\omega\eta \tag{56}$$

where, η is the free surface elevation; h is the water depth and k is the wave number.

To absorb the incident waves in right hand side of the NWT an open boundary condition was applied (Contento, 2000) as [27]:

$$V_{OpenBoundary} = g\eta\frac{k}{\omega} \tag{57}$$

All outgoing waves are absorbed at open boundary and there is no reflection in the right hand side of NWT. It should be noted that damped waves mostly behave in a linear way in this system. Figure 6 shows monitoring profile of waves at the right hand side of the flume and its comparison with the linear wave theory. It is seen that it is very close to the linear wave.

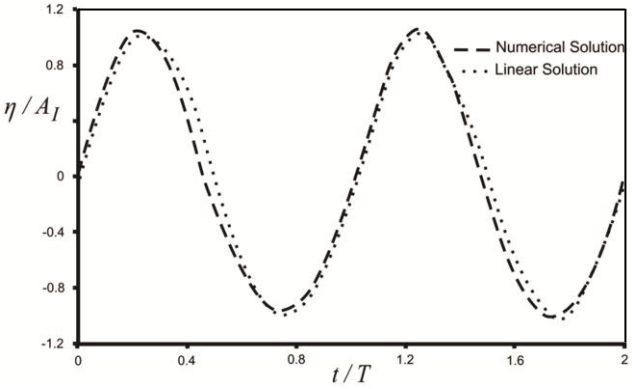

Figure 6. Comparison between numerical and analytical results based on linear solution;

5. Results

In order to assess the accuracy and validity of the numerical model, results of generated linear waves and their interaction with a vertical porous structure were compared with the available data.

5.1. Wave Verification

In this section numerical wave tank with a length of 15m, a height of 0.81m and a depth of 0.5m was considered. Generated waves by piston type wavemaker had amplitude of 0.03 m and a period of 1.2s.

Three grids in the x and y directions were selected as Table1 for wave generation in numerical model.

Table 1. Different mesh sizes for wave generation in numerical model

	δy [cm]	δz [cm]
Grid I	1	0.5
Grid II	2	1
Grid III	3	1.5

The results are presented in Figure 8. It is evident from this figure that there is a good agreement between numerical results with three different grids and that of linear wave. Therefore Grid I was applied in this study for all wave numerical modeling.

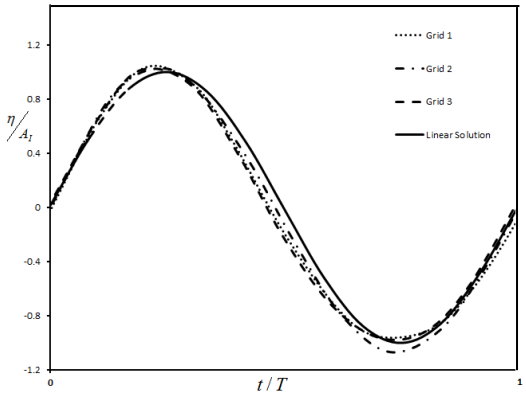

Figure 8. Comparison between numerical and analytical results based on linear solution;

5.2. Validation of Wave–Structure Interaction Results

The height of damped waves in the rear wall of a vertical porous breakwater was estimated by Karim et al. (2003) using numerical model [8]. In their study extended Navier-Stokes equations and VOF method were implemented assuming viscous flow. In the present study their results were used to validate the model for wave and porous medium interaction. Wave height damping was studied for different breakwater widths for a 0.07m height, 1.6 s period incident wave in a NWT. Figure 9 shows this test schematically. The medium porosity, drag and inertia coefficients were selected as 0.6, 3.5 and 0.5 respectively to be consistent with those of Karim et al. tests.

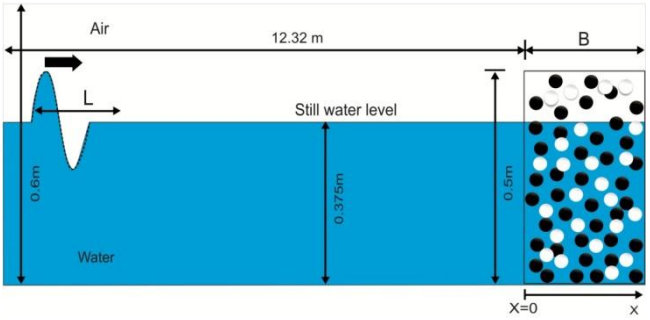

Figure 9. Schematic view of Karim et al. numerical wave channel with porous structure;

Figure 10 shows comparison of the present work and Karim et al. numerical results. The present work seems to have more accurate results.

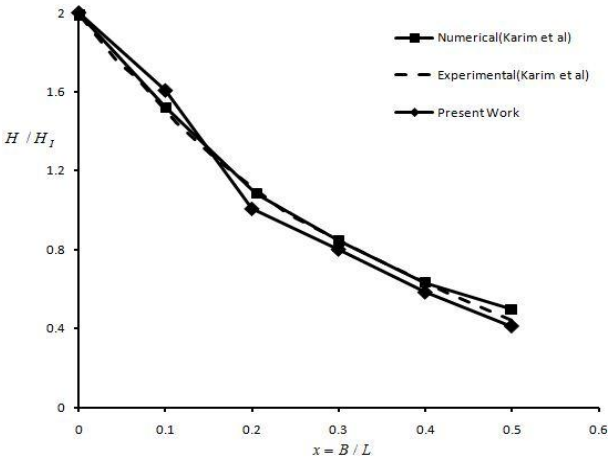

Figure 10. Comparison of present work results and those of Karim et al. (2003) for damped wave heights in the rear wall of a vertical porous breakwater;

5.3. Results of Wave Interaction with a Submerged Breakwater

Schematic of the submerged breakwater in the numerical wave tank is shown in Figure 11. The inertia and drag coefficients were assumed to be 1.2 and 2.5 consistent with Hieua and Tanimoto [14] with a porosity of 0.5. The incident wave had a period and amplitude of 1.2s and 0.06m respectively. The breakwater crest width was selected as a multiple of wave length λ.

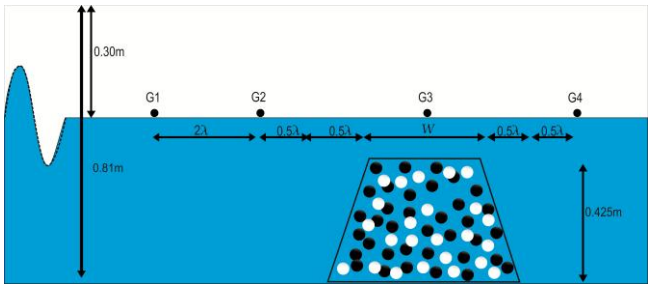

Figure 11. Schematic view of the numerical wave tank with submerged rubble mound breakwater;

The wave elevations were recorded in four different gauges and results are presented in Figure 12. This figure shows that the wave height increases as the wave reaches on the crest of the submerged breakwater.

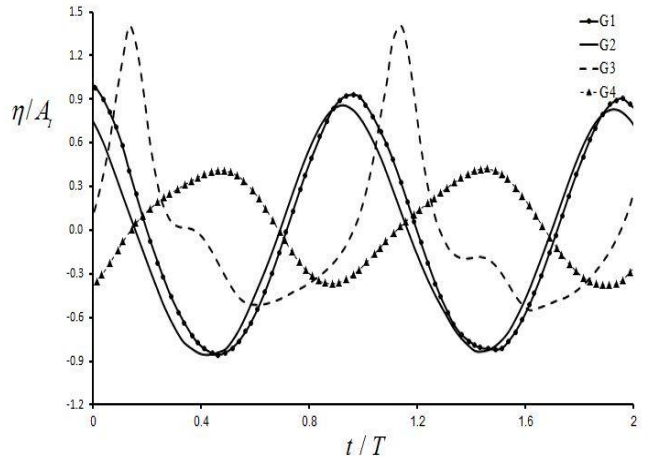

Figure 12. Time histories of free surface elevation recorded at different probes for constant CD=2.5 and CM=1.2;

In the first step the transmitted wave time histories were considered for different incident wave amplitudes. Figure 13 shows non-dimensional amplitude of transmitted waves at G4 against non-dimensional time for different incident wave amplitudes. It is evident from this figure that when the incident wave height increases the transmitted wave amplitude decreases.

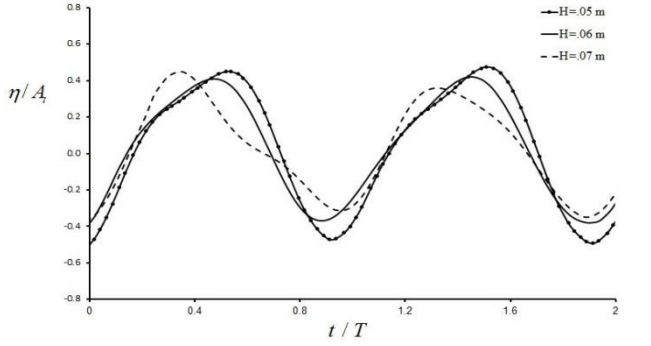

Figure 13. Time histories of free surface elevation recorded at G4 for different heights of incident waves;

In the next step the effect of incident wave period on transmitted waves was considered. Figure 14 shows non-dimensional amplitude of transmitted waves at point G4 against non-dimensional time for different incident wave periods but a constant height of 0.06 m. It can be seen that as the incident wave period increases the phase shift between transmitted waves also increases in the form of time lag.

In order to study the effect of drag coefficient on wave damping, three different drag coefficients were selected. Figure 15 shows the effect of drag coefficient on transmitted wave damping. As shown in this figure, for three different drag coefficients of 2.1, 2.5 and 2.9 there is no major different in damping of transmitted waves.

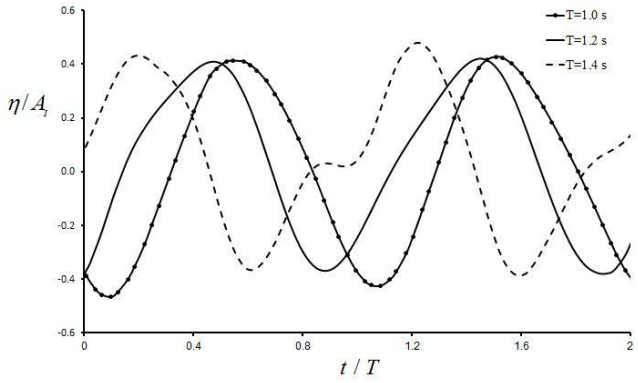

Figure 14. Time histories of free surface elevation recorded at G4 for different periods of incident waves;

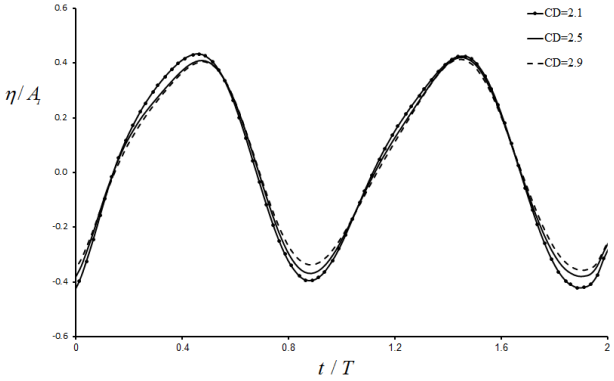

Figure 15. Time histories of free surface elevation of waves recorded at G4 for different drag coefficients;

To consider the effect of inertial term, different inertia coefficients were exerted to the numerical model. Figure 16 shows the time histories of transmitted waves for CM= 0.8, 1.2 and 1.6. It is clear from this figure that wave attenuation is almost the same for different inertia coefficients. However a phase shift exists for different inertia coefficients.

To consider the effect of porosity of the structure on the transmitted waves different porosities as n= 0.4, 0.5 and 0.6 were selected. The results are presented in Figure 17. This figure shows that there is a direct relationship between phase delay of transmitted waves and porosity of the structure.

It is also evident in these figures that waves passing the breakwater somehow have a fluctuating nature. This phenomenon shows that this attenuation needs more time to be established. In Figure 16 the variable parameter is inertia force which in turn generates negative acceleration against propagating wave and this leads to requiring more time to reach to the same wave profile. In Figure 17 with decreasing the porosity more wave blockage in the left hand side of the breakwater occurs and therefore the variation of wave height in right hand side of the breakwater is more considerable. It is due to wave's shock attenuation which damps faster as porosity decreases and vice versa.

The effect of crest height on damping of waves was studied using three different crest heights of 38.25 cm; 44.25 cm and 50.25 cm. The corresponding crest water depths were 12.75 cm; 6.75 cm and 0.75 cm respectively (see Figure 18). Considering a constant base width for the breakwater the slope of the structure changed accordingly to its height.

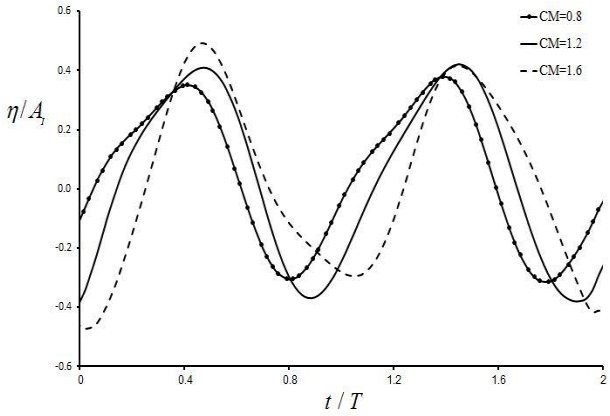

Figure 16. Time histories of free surface elevation of waves recorded at G4 for different inertia coefficients;

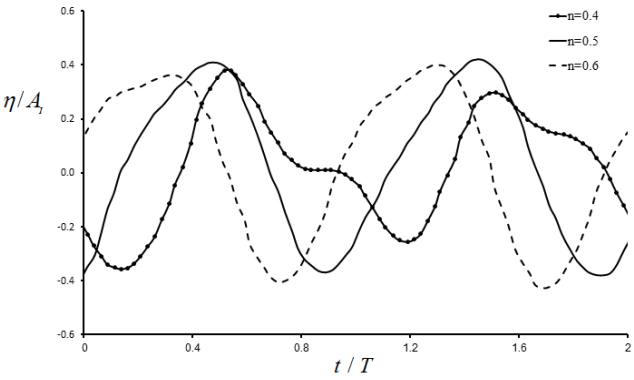

Figure 17. Time histories of free surface elevation of waves recorded at G4 for different porosity coefficients;

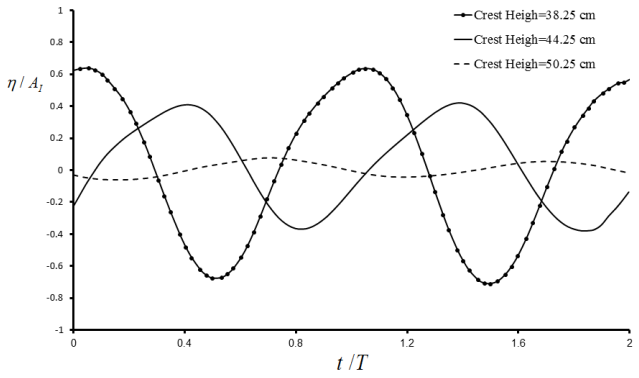

Figure 18. Time histories of free surface elevation of waves recorded at G4 for different crest heights;

6. Discussion and Conclusions

In this paper a modified numerical model was developed to simulate the waves and porous structure interaction. On the basis of viscous flow assumption and using the modified Navier-Stokes equations, the hydrodynamic performance of the porous structure was assessed using the Cut-Cell method. The present model was validated by comparison of damped wave heights results in the rear wall of a vertical porous structure with available data. Further tests showed that as the waves passing over the submerged breakwater, the wave height increases in the middle of structure. However, as the waves propagate further in the structure, the wave height decreases. This phenomenon can be justified as inflow area of the structure dramatically decreases. The numerical results also show that increasing of height or period of the incident waves can lead to a time lag between incident and transmitted waves. This is also reasonable as the incident waves height or period increases the porous media would dissipate it more efficiently and this gives rise to more delay on wave propagation. Studies on the drag and inertia coefficients revealed that drag coefficient does not play an important role on the rate of transmitted waves. However increasing of inertia coefficient is associated with more time lags for the incident waves passing the breakwater. This can be related to extra momentum which is needed to accelerate a given volume of water inside the porous medium relative to pure water. Decreasing of the porosity causes more attenuation on incident wave leading to more phase shift between the incident and transmitted waves. This result could be explained considering the sudden reduction of inflow area in the breakwater. Reduction of porosity also results in rise of drag and inertia forces against propagation of incident waves. The studies on effect of submerged breakwater crest width on the transmitted waves shows that a double crest width causes a decrease to transmitted wave height of about 40%. While an increase of 30% on crest height causes a decrease of 80% on transmitted wave height.

6. References

1- Vílchez, M., Clavero, M., Losada, Miguel A., (2015), *Hydraulic performance of different non-overtopped breakwater types under 2D wave attack*, Journal of Coastal Engineering , Vol. 107, p. 34-52.

2- Jensen, B., Niels Gjøl, J., (2104). *Investigations on the porous media equations and resistance coefficients*, Journal of Coastal Engineering, Vol. 84, p. 56-72.

3-Liu, Y., Li, H-J., (2013), *Wave reflection and transmission by porous breakwaters: A new analytical solution*, Journal of Coastal Engineering, Vol.78, p. 46–52.

4-Yang, C., Lu, H.D., Löhner, R., (2010), *On the simulation of highly nonlinear wave-breakwater interactions*, Journal of Hydrodynamics, Ser. B Vol. 22, p. 975–981.

5-Wu, Y-T., Hsiao, S-C., (2013), *Propagation of solitary waves over a submerged permeable breakwater*, Journal of Coastal Engineering Vol. 81, p. 1–18.

6-Hieu, P.D., Vinh, P.N., (2013), *Numerical study of wave overtopping of a seawall supported by porous structures*, Journal of Applied Mathematical Modelling Vol. 36, p. 2803–2813.

7-Mendez, F.J., Losada, I., Losada, M., (2001), *Wave-induced mean magnitudes in permeable submerged breakwaters*. Journal of Waterway, Port, Coastal, and Ocean Engineering, Vol. 127, p. 7-15.

8-Karim, M.F., Tanimoto, K., Hieu, P.D., (2003), *Simulation of wave transformation in vertical permeable structure.* Journal of International Offshore and Polar Engineering Conference, p. 729-735.

9-Karim, M.F., Tanimoto, K., Hieu, P.D., (2009), *Modeling and simulation of wave transformation in porous structures using VOF based two-phase flow model.* Journal of Applied Mathematical Modeling, Vol. 33, p. 343-360.

10-Zhang, J.S., Jeng, D.S., Liu, P.L.F., (2011), *Numerical study for waves propagating over a porous sea bed around a submerged permeable breakwater PORO-WSSIII model*. Journal of Ocean Engineering, Vol. 38, p. 954–966.

11-Guta, L., Sundar, S., (2010), *Navier-Stokes-Brinkman system for interaction of viscous waves with a submerged porous structure.* Journal of Tamkang Journal of Mathematics, Vol. 41, p. 217-243.

12-Zhao, Q., Armfield, S., Tanimoto, K., (2004), *Numerical simulation of breaking waves by a multi-scale turbulence model.* Journal of Coastal Engineering, Vol. 51, p. 53-80.

13-Garcia, N., Lara, J.L., Losada, I.J., (2004), *2-D numerical analysis of near-field flow at low-crested permeable breakwaters.* Journal of Coastal Engineering, Vol. 51, p. 991– 1020.

14-Hieu, P.D., Tanimoto, K., (2006), *Verification of a VOF-based two-phase flow model for wave breaking*

and wave–structure interactions. Journal of Ocean Engineering, Vol. 33, p. 1565–1588.

15-Lynett, P.J., Liu, P.L.F., Losada, I.J., Vidal, C., (2000), *Solitary wave interaction with porous breakwaters*. Journal of Waterway, Port, Coastal, and Ocean Engineering Vol. 127, p. 314-322.

16-Lara, J.L., Garcia, N., Losada, I.J., (2006), *RANS modeling applied to random wave interaction with submerged permeable structures*, Journal of Coastal Engineering, Vol. 126, p. 395–417.

17-Karim, M.F., Tingsanchali, T.A., (2006), *Coupled numerical model for simulation of wave breaking and hydraulic performances of a composite seawall.* Journal of Ocean Engineering, Vol. 33, p.773–787.

18-Seifollahi, M., Shirani, E., Ashgriz, N., (2008), *An improved method for calculation of interface pressure force in PLIC-VOF methods.* European Journal of Mechanics B/Fluids, Vol. 27, p. 1-23.

19-Tucker, P.G., Pan, Z.A., (2000), *Cartesian cut cell method for incompressible viscous flow*, Journal of Applied Mathematical Modeling, Vol. 24, p. 591-606.

20-Luo, X.L., Gu, Z.L., Lei, K.B., Wang, S., Kase, K.A., (2012), *Three-dimensional Cartesian cut cell method for incompressible viscous flow with irregular domains*, International Journal for Numerical Methods in Fluids, Vol. 69, p. 1939–1959.

21-Kirkpatrick, M.P., Armfield, S.W., Kent, J.H., (2003), *A representation of curved boundaries for the solution of the Navier–Stokes equations on a staggered three-dimensional Cartesian grid*, Journal of Computational Physics, Vol. 184, p. 1-36.

22-Kim, H.J., Lee, J.W., Cho, Y.S., (2010), *Numerical simulation of shallow-water flow using a modified Cartesian cut-cell approach*, Journal of Engineering Mechanics (ASCE), Vol. 136, p. 399–404.

23-Kondo, A., Huang, Y., Maeda, K., (2013*), DEM coupled SMAC simulation on the moving Process of flow like landslide*, Journal of New Frontiers in Engineering Geology and the Environment, Vol. 9, p.195-198.

24-Zhang, J., Zheng, J., Jeng, D-S., Wang, G., (2012), *Numerical simulation of solitary wave induced flow motion around a permeable submerged breakwater*. Journal of Applied Mathematics, p. 1-14.

25-He, X., Liu, N., Li, S., Wang, H., Wang, G., (2012), *Local Poisson SPH for Viscous Incompressible Fluids.* Journal of Computer Graphics Forum, Vol. 31, p. 1948–1958.

26-Katell, G., Eric, B., (2002), *Accuracy of solitary wave generation by a piston-wave make.* Journal of Hydraulic Research, Vol. 40, p. 321-331.

27-Contento, G., (2000), *Numerical wave tank computations of nonlinear motions of two-dimensional arbitrarily shaped free floating bodies*, Journal of Ocean Engineering, Vol. 27, p. 531–556.